

A Method for Identifying Farmland System Habitat Types Based on the Dynamic-Weighted Feature Fusion Network Model

Kesong Zheng^{a,#}, Zhi Song^{b,#}, Peizhou Li^{c,#}, Shuyi Yao^d, Zhenxing Bian^{d,*}

*Corresponding author: Zhenxing Bian : zhx-bian@syau.edu.cn

Kesong Zheng : kesong.zheng@qq.com

Zhi Song : zhisong@syau.edu.cn

Peizhou Li : 2023107094@stu.syau.edu.cn

Shuyi Yao : 540241263@qq.com

^a Changjiang Institute of Technology, Wuhan, Hubei, 430212 China

^b College of Science, Shenyang Agricultural University, Shenyang, Liaoning, 110866 China

^c College of Engineering, Shenyang Agricultural University, Shenyang, Liaoning, 110866 China

^d College of Land and Environment, Shenyang Agricultural University, Shenyang, Liaoning, 110866 China

[#] These authors contributed equally to this work and should be considered co-first authors.

Abstract: Addressing the current lack of a standardized habitat classification system for cultivated land ecosystems, incomplete coverage of habitat types, and the inability of existing models to effectively integrate semantic and texture features—resulting in insufficient segmentation accuracy and blurred boundaries for multi-scale habitats (e.g., large-scale field plots and micro-habitats)—this study developed a comprehensively annotated ultra-high-resolution remote sensing image dataset encompassing 15 categories of cultivated land system habitats. Furthermore, we propose a Dynamic-Weighted Feature Fusion Network (DWFF-Net). The encoder of this model utilizes a frozen-parameter DINOv3 to extract foundational features. By analyzing the relationships between different category images and feature maps, we introduce a data-level adaptive dynamic weighting strategy for feature fusion. The decoder incorporates a dynamic weight computation network to achieve thorough integration of multi-layer features, and a hybrid loss function is adopted to optimize model training. Experimental results on the constructed dataset demonstrate that the proposed model achieves a mean Intersection over Union (mIoU) of 0.6979 and an

F1-score of 0.8049, outperforming the baseline network by 0.021 and 0.0161, respectively. Ablation studies further confirm the complementary nature of multi-layer feature fusion, which effectively improves the IoU for micro-habitat categories such as field ridges. This study establishes a habitat identification framework for cultivated land systems based on adaptive multi-layer feature fusion, enabling sub-meter precision habitat mapping at a low cost and providing robust technical support for fine-grained habitat monitoring in cultivated landscapes.

Keywords: DINOv3 ; Multi-level feature fusion ; dynamic weighting ; cultivated land system habitat dataset ; habitat type identification ; semantic segmentation

1.Introduction

Agricultural intensification has exacerbated landscape homogenization, leading to global ecological challenges such as the degradation of ecological functions in croplands and the decline of farmland biodiversity (Delabre et al. 2021). Recent research has shifted focus toward semi-natural habitats within agricultural landscapes—land types not under conventional cultivation but possessing critical ecological functions, such as shelterbelts, grasslands, ponds, field margins, ditches, road edges, and fallow lands. These areas are collectively referred to as non-crop habitats and serve as key reservoirs for enhancing biodiversity and ecosystem services within cultivated land systems (Jingping et al. 2022). They play a vital ecological role in agricultural landscapes (Tougeron et al. 2022). The appropriate spatial configuration of non-crop habitats is a sustainable approach to balancing agricultural intensification and biodiversity conservation. Maintaining about 20% - 30% of such habitats can sustain diverse and stable farmland biodiversity (Zhang et al. 2024), while linear elements around fields enhance landscape connectivity and ecological network stability (Wang et al. 2024). Together with cultivated areas, non-crop habitats form an integrated ecological-economic complex known as the cultivated land system. As crucial spatial entities for sustaining biodiversity in agricultural land, non-crop habitats exhibit diverse forms depending on their spatial distribution, shape, vegetation type, and characteristics, thereby creating a heterogeneous landscape pattern (Guo et al. 2020; Y. Zhang et al. 2025). Therefore, accurate identification of habitats within the cultivated land system—particularly the types and boundaries of non-crop habitats—is essential for quantitative research on ecological management and conservation of cultivated lands (Tulczyjew et al. 2022).

The accurate identification of habitats within cultivated land systems requires a comprehensive consideration of multiple dimensions, including land cover types,

spatial configuration, morphological characteristics, and vegetation attributes, which in turn demands high-quality annotated datasets for support. However, most existing mainstream datasets (e.g., Potsdam and Vaihingen) are predominantly designed for urban scenarios (Song et al. 2023), and lack high-quality annotations tailored to habitat types in complex agricultural landscapes (Sumbul et al. 2021). The construction of such specialized datasets faces several challenges. First, the habitat types in cultivated land systems are diverse and complex, often characterized by small target sizes and intricate boundaries. Second, a standardized habitat classification system has yet to be established, resulting in the absence of unified criteria and a systematic framework. Third, the spatial resolution of remote sensing imagery is often insufficient to capture fine-scale habitat details, and there exists a trade-off between patch size and habitat connectivity. Finally, it remains difficult to acquire representative, high-quality samples that comprehensively cover major habitat types.

At the technical level, the accurate extraction of topographic transition zones narrower than 5 m is often hindered by the mixed pixel effect, a limitation inherent in medium- and low-resolution remote sensing imagery (Yuan, Shi, and Gu 2021). Furthermore, traditional remote sensing techniques exhibit limited performance in classifying structurally complex or fine-scale habitats, with reported accuracies falling below 65% (Liu and Gong 2021), thereby failing to meet the high demands for precise micro-habitat identification and boundary delineation. The advent of very high-resolution (VHR) remote sensing imagery offers a novel technical approach for the fine-scale identification and monitoring of cultivated land habitats. In recent years, deep learning-based interpretation of high-resolution remote sensing imagery has emerged as a predominant research focus (Zhou et al. 2021). Pioneering deep learning models, including FCN (Farhangfar and Rezaeian 2019), CNN (Kalchbrenner, Grefenstette, and Blunsom 2014), U-Net (Azad et al. 2024) and DeepLab (Chen et al. 2018), have significantly advanced semantic segmentation performance through their end-to-end architectures. While their application to VHR image-based field extraction tasks has improved geometric accuracy, these methods often fall short in fully integrating multi-level semantic information, leading to incomplete extraction of land parcels. While existing studies have demonstrated the accuracy of deep learning in extracting large-scale contiguous objects (Zhang et al. 2022), its application in agricultural landscape habitats presents greater challenges. Such environments exhibit a wider variety of types and more complex boundary structures, requiring simultaneous attention to both macro-scale features (e.g., field

patches) and micro-scale elements (e.g., field margins). Moreover, issues of mixed pixels and boundary ambiguity are considerably more severe in these contexts compared to the scenarios previously studied.

In summary, this study aims to address three core scientific issues:

(1) constructing a comprehensively categorized and finely annotated dataset for cultivated land system habitats;

(2) developing an efficient habitat feature extraction network;

(3) By designing a dynamic weighted multi-layer feature fusion network, the semantic and texture information are effectively integrated to improve the segmentation accuracy of cultivated land system habitat.

To this end, the study proposes the construction of a ultra-high-resolution remote sensing image dataset tailored to cultivated land system habitats, along with a Dynamic Weight Feature Fusion Network (DWFF-Net) model. The objective is to achieve precise and efficient identification of cultivated land system habitats under ultra-high-resolution remote sensing conditions, while striving to significantly improve both the accuracy and robustness of habitat recognition—all within manageable model complexity and computational costs.

2.Related work

2.1 Semantic Segmentation in Agricultural Remote Sensing

Semantic segmentation of agricultural scenes using drone imagery has consistently been a focus of research (Z. Zhang et al. 2025; Zualkernan et al. 2023) . Early approaches primarily relied on traditional machine learning techniques such as support vector machines (SVM) and random forests. With the rise of deep learning, convolutional neural network (CNN)-based architectures have gradually become dominant (Sheppard and Rahmehoonfar 2017). Among these, U-Net, with its symmetric encoder–decoder structure and skip connections, has emerged as an industry standard and inspired numerous variants specifically designed for remote sensing applications (Peng et al. 2024). Architectures such as DeepLabv3+ further improved performance by incorporating dilated convolutions, which help maintain feature resolution while expanding the receptive field (Cao et al. 2024). Although these methods perform well in segmenting large homogeneous regions such as crop fields, they often struggle to preserve fine details of small-scale linear structures, largely due to the frequent use of pooling or strided convolution operations.

2.2 Vision Transformers for Semantic Segmentation

The remarkable success of Transformer models in natural language processing

has facilitated its expansion into the field of computer vision (Vaswani et al. n.d.). Vision Transformer (ViT). The Vision Transformer (ViT) demonstrated that a pure Transformer architecture, by decomposing an image into a sequence of patches, can also achieve competitive performance. Subsequent research has extended ViT to dense prediction tasks such as semantic segmentation. For instance, SegFormer combines a hierarchical ViT encoder with a lightweight multilayer perceptron (MLP) decoder, achieving a balance between performance and efficiency (Fan et al. 2024). Mask2Former further unifies semantic, instance, and panoptic segmentation under a mask classification paradigm (Qiao et al. 2023). While these models exhibit considerable potential, they typically require full fine-tuning on large-scale annotated datasets, which can be prohibitively expensive in domain-specific scenarios.

2.3 Vision Foundation Models and Self-Supervised Learning

Visual foundation models represent a paradigm shift toward general-purpose visual understanding. Models such as DINO, DINOv2, and DINOv3 are pre-trained on large-scale unlabeled image datasets via self-supervised objectives (e.g., label-free knowledge distillation (Li et al. 2025)), enabling them to learn highly robust and semantically rich representations. A key characteristic of these models is their ability to maintain exceptional performance even when used as frozen feature extractors (Siméoni et al. 2025). The DINOv3 paper particularly highlights two properties relevant to our work: (1) the ability to generate clear, high-quality dense feature maps that remain stable even under very high input resolutions, and (2) the incorporation of “Gram anchoring” during pre-training to mitigate degradation in patch-level consistency. Building directly upon these properties, our study aims to design a decoder that fully leverages the advantages of high-resolution feature fidelity and effectively integrates the structural information of features.

3. Methodology

Figure 1 depicts the overall architecture of the proposed DWFF-Net. This framework utilizes a frozen DINOv3 encoder as its backbone for feature extraction, integrated with a novel decoder that features a Dynamic Weight Feature Fusion (DWFF) mechanism to produce the final segmentation map. The model is optimized end-to-end via a composite loss function, formulated by integrating an L2-regularized hybrid segmentation loss with the summation of weight entropy across multi-level features.

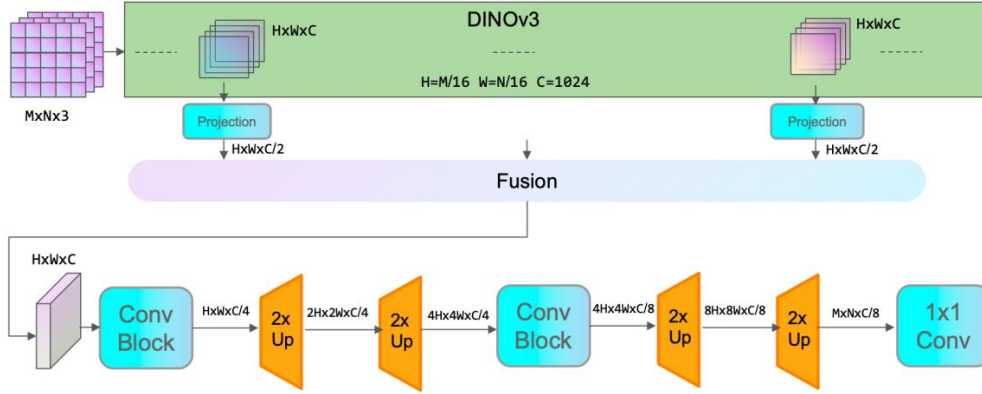


Figure 1 Overall architecture of the proposed DWFF-Net model for farmland system habitat type identification.

3.1 DINOv3 as a Frozen Multi-Level Feature Extractor

We leverage DINOv3 with a Vision Transformer Large backbone and a patch size of 16 (DINOv3-ViT-L/16) as a frozen multi-level feature extractor. The ViT architecture processes an input image $I \in \mathbb{R}^{H \times W \times 3}$ by first dividing it into a sequence of non-overlapping patches, which are subsequently linearly projected into patch embeddings. These embeddings are then propagated through a cascade of Transformer blocks to generate hierarchical feature representations.

A fundamental aspect of our approach is that the entire DINOv3 backbone remains frozen throughout the training process. This design offers several key benefits: (1) it substantially reduces the number of trainable parameters, thereby accelerating convergence and lowering memory consumption; (2) it helps prevent overfitting, which is particularly relevant given the limited scale of specialized remote sensing datasets compared to large-scale pre-training data; and (3) it encourages the decoder to learn how to effectively interpret the rich and general-purpose representations from the foundation model, rather than altering its pre-trained feature space.

3.2 Decoder Design

The Dynamic-Weighted Feature Fusion Network Decoder (DWFF) is designed to efficiently integrate multi-scale features extracted from the DINOv3 encoder. It aims to combine the precise spatial localization information provided by shallow features with the semantically rich contextual cues captured by deeper layers. The architecture of the decoder comprises three core components: projection, fusion and Dynamic-Weighted Network.

3.2.1 Feature Projection

Given that features originating from different layers in a Vision Transformer (ViT) possess identical channel dimensions, we first project each feature map F_i

into a shared low-dimensional subspace via a 1×1 convolution. This operation is followed by Group Normalization and a ReLU activation function. Such projection not only reduces computational complexity but also facilitates the learning of task-specific feature representations.

$$F'_i = \text{ReLU}(\text{GN}(\text{Conv}_{1 \times 1}(F_i))) \in \mathbb{R}^{B \times C_{fus} \times H_p \times W_p}$$

where C_{fus} is the fusion channel dimension and (H_p, W_p) are the patch dimensions of the feature map.

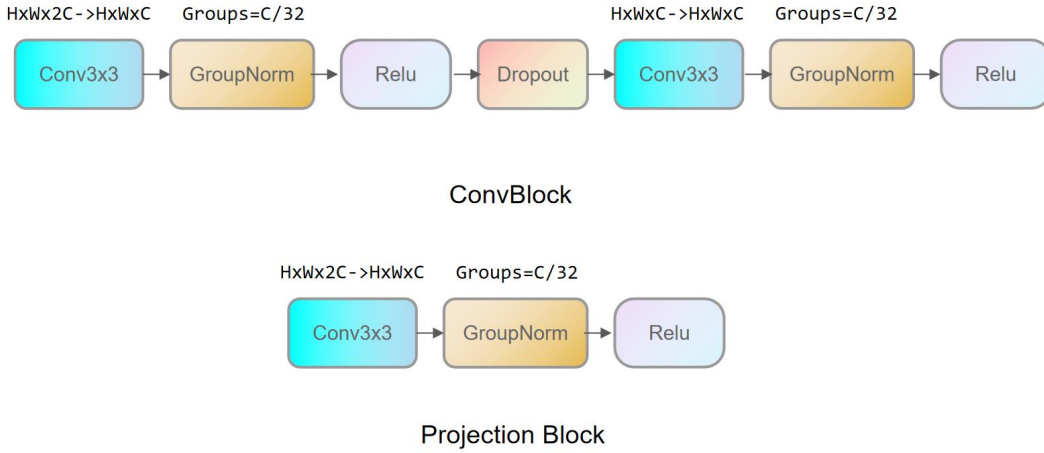


Figure 2 Schematic diagram of the feature projection.

3.2.2 Dynamic-Weighted Feature Fusion Network (DWFF)

We initially developed a global weighted feature fusion network, termed Static-Weighted Feature Fusion Network (SWFF-Net), which enhances the utilization of multi-level features to some extent by integrating hierarchical features using predefined fixed weights.

Different feature layers emphasize distinct aspects of habitat information in cultivated land systems, ranging from low-level texture information (Layer 1) to high-level semantic information (Layer 24). However, the simple SWFF-Net model, when fusing these multi-scale features, relies solely on a set of static global weights and fails to adequately account for the dynamic variations in information content across different feature layers under varying input samples. To address this limitation, we further propose a dynamic weighted feature fusion network model, named Dynamic-Weighted Feature Fusion Network (DWFF-Net). By incorporating an input-driven adaptive weight allocation strategy, this model achieves dynamic calibration of the information contained in different feature layers, thereby enabling more effective fusion of multi-level feature information.

As Figure 3, a learnable weight generation mechanism is employed to adaptively fuse features across levels. Specifically, each level's feature undergoes global average pooling (GAP) to produce a compact vector, which are then concatenated. A two-layer MLP (with ReLU activation) processes the concatenated vector to generate level-wise scores. These scores are normalized via softmax with a learnable temperature parameter, yielding normalized weights for each level.

Consequently, the unified fused feature generated by the proposed dynamic weighting network is expressed as F_{fus} :

$$F_{fus} = \sum_{i=1}^m \xi_i * F_i$$

where m denotes the number of feature layers selected for fusion, and ξ_i represents the weight assigned to each layer after Softmax normalization.

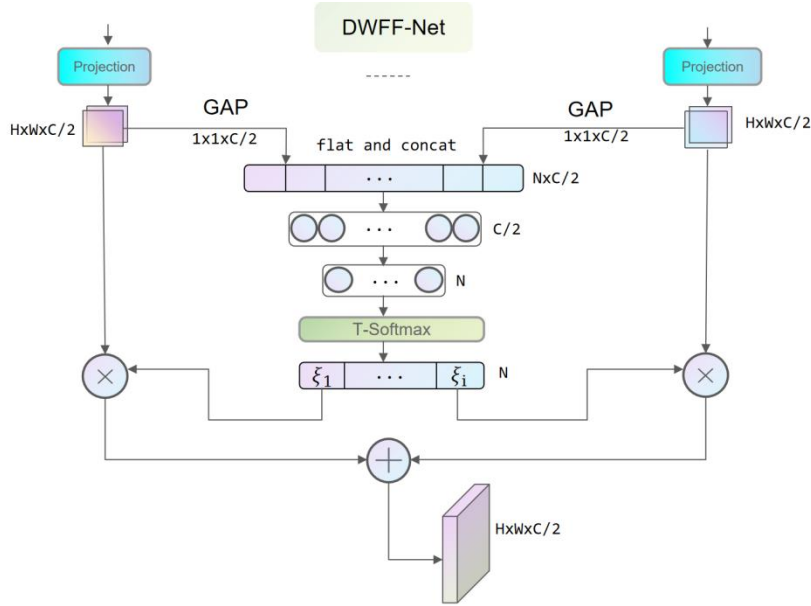


Figure 3 Dynamic-Weighted Feature Fusion (DWFF) mechanism for integrating multi-scale features.

3.3 Overall Loss Function

As a central component of the supervised learning framework, the loss function not only serves as an objective function guiding parameter updates but also acts as a performance evaluation metric that drives feature learning. In this study, we propose a novel composite loss function architecture:

$$L_{total} = L_{seg} + \lambda_1 L_{L2} - \lambda_2 L_{entropy}$$

Here, λ_1 and λ_2 are two adjustment coefficients, which are assigned values of 0.04 and 0.01, respectively, in this study.

To combat the widespread issue of severe class imbalance commonly encountered in agricultural imagery, we implemented a hybrid loss function integrating Dice loss and Focal loss.

$$L_{seg} = \alpha L_{Dice} + \beta L_{Focal}$$

In this study, we design a composite loss function, L_{seg} , which effectively integrates the global region optimization capacity of the Dice loss (L_{Dice}) with the hard sample focusing capability of the Focal loss (L_{Focal}). The coefficients α and β serve as balancing hyperparameters for the respective loss components. This formulation ensures that the segmentation network maintains the overall structural consistency of target regions while precisely capturing their fine boundary details throughout the training process.

The Dice loss was originally derived from binary tabular data analysis. By enhancing gradient responses for small-scale target structures, the constructed loss function improves regional consistency, making it particularly effective for capturing fine-grained features in habitat classification tasks. The formula for Dice loss is as follows:

$$L_{Dice} = \frac{2|X \cap Y|}{|X| + |Y|}$$

In this equation, $|X|$ and $|Y|$ denote the binary masks of the ground truth and the predicted segmentation, respectively.

The Focal loss function effectively emphasizes hard examples, such as those in shadowed regions, by automatically assigning higher weights to low-confidence samples, thereby mitigating class imbalance. The formulation of the Focal loss is provided as follows:

$$L_{Focal} = -\alpha_t (1 - p_t)^\gamma \log(p_t)$$

In the equation, p_t denotes the predicted probability of the target class by the model; α_t is a balancing factor that adjusts the influence between positive and

negative samples; and γ is the focal factor, which modulates the weight assigned to hard and easy examples, thereby enhancing the model’s focus on challenging cases and improving its overall calibration.

The introduction of the L2 regularization term L_{L2} enhances the robustness of the optimization process, particularly in high-dimensional scenarios where overfitting is frequently encountered. By discouraging excessively large weight values, this regularization term promotes model simplicity, improves generalization capability, and reduces variance without substantially increasing bias. The formulation of L_{L2} is given as follows:

$$L_{L2} = \sum_i \omega_i^2$$

In the equation, ω_i denotes an individual weight parameter of the model, while λ represents a hyperparameter that controls the strength of regularization.

To ensure the accuracy of multi-layer fusion and prevent weight collapse, the total entropy of each feature layer in the DINOv3 network must be calculated, denoted as $L_{entropy}$, is introduced. Entropy serves as a metric for the uniformity of a probability distribution: a higher entropy value indicates a more uniform weight distribution (e.g., when all weights are 0.25, entropy reaches its maximum), whereas a lower entropy value suggests a more concentrated distribution (e.g., when one weight approaches 1 while others are close to 0). By subtracting the $L_{entropy}$ term from the total loss function, the aim is to mitigate the issue of excessively concentrated weight distributions. Since the loss function is optimized toward minimization, a smaller entropy value (which contributes more due to the negative sign) leads to a larger total loss and consequently generates stronger gradients. During gradient descent, this drives the model to adjust its parameters in a way that increases entropy, thereby promoting a more uniform weight distribution.

The selection of feature layers is designed to capture multi-scale representations, spanning from low-level textures (Layer 1) to high-level semantic information (Layer 24). Taking into account both computational complexity and experimental constraints, four specific layers—namely, Layers 1, 8, 16, and 24—were systematically sampled, and the sum of their information entropy was computed. The formulation of the entropy loss term, $L_{entropy}$, is given as follows:

$$L_{entropy} = -\sum p_i(x) \log p_i(x)$$

In the equation, $p_i(x)$ represents the probability distribution derived from the normalized feature activations of a specific layer.

3.4 Weight collapse

In Section 3.2, we developed the DWFF-Net architecture, which employs a data-driven strategy to dynamically generate weights for feature fusion. During the training process, however, the attention mechanism may disproportionately and persistently favor a narrow subset of features—such as those from specific layers or channels—leading to a phenomenon termed “attention dictatorship.” This issue induces weight collapse, wherein a limited number of features dominate the attention distribution, while the contributions of other potentially informative features are significantly suppressed. Consequently, the performance gains that the attention mechanism is intended to deliver are undermined.

The $L_{entropy}$ introduced in Section 3.3 partially addresses this phenomenon, and further mitigation is required., a temperature hyperparameter ($temp$) is introduced to modulate the original attention scores. Specifically, the final attention weights are computed by applying a softmax function to the temperature-scaled scores:

$$Weight = F_{\text{softmax}}\left(\frac{scores}{temp}\right)$$

This temperature parameter functions as a smoothing factor for probability distribution, effectively controlling the degree of weight distribution smoothing and entropy. When the temperature is high ($temp > 1$), the weight distribution becomes more uniform, enhancing the model's ability to explore different feature layers. Conversely, low-temperature settings ($temp < 1$) amplify the weights of highly scored features, resulting in a more concentrated distribution. By appropriately adjusting the temperature, we can mitigate attentional bias caused by weight distribution polarization, facilitate effective fusion of multi-source features, and improve the model's representational capabilities and generalization performance.

3.5 Model Performance Evaluation

The evaluation of semantic segmentation algorithms generally adheres to well-established conventions in the computer vision field, utilizing metrics such as

Precision, Recall, F1-score, and Intersection-over-Union (IoU). In binary classification tasks, each pixel is typically categorized into one of four classes: True Positive (TP), True Negative (TN), False Positive (FP), and False Negative (FN). The relevant performance metrics are defined as follows:

$$Precision = \frac{TP}{TP + FP}$$

$$Recall = \frac{TP}{TP + FN}$$

$$F1 = \frac{2 \times Precision \times Recall}{Precision + Recall}$$

$$IoU = \frac{TP}{TP + FP + FN}$$

To comprehensively evaluate and compare the overall performance of different models, we introduce the following metrics: mean Precision (mPrecision), mean Recall (mRecall), mean F1-score (mF1), and mean Intersection over Union (mIoU). The corresponding formulas are provided below.

$$mPrecision = \frac{\sum_{i=1}^{15} Precision_i}{15}$$

$$mRecall = \frac{\sum_{i=1}^{15} Recall_i}{15}$$

$$mF1 = \frac{\sum_{i=1}^{15} F1_i}{15}$$

$$mIoU = \frac{\sum_{i=1}^{15} IoU_i}{15}$$

4. Experiments and result

4.1 Dataset

The experimental area was located in the Hailun River Basin of Hailun City, Heilongjiang Province, China (Figure 4), spanning from 47°19'N to 47°27'N and 126°44'E to 126°57'E. With an average elevation of 201 m and a total area of 74.1

km², the region is characterized by gently rolling hills (manchuan mangang landform). The primary crops cultivated include maize and soybean. The farmland is often interspersed with shelterbelts, grass strips, and gullies, contributing to a diverse array of habitats within the agricultural landscape.

The ultra-high-resolution remote sensing imagery utilized in this study was acquired by the FeimaRobotics V500 vertical take-off and landing fixed-wing unmanned aerial vehicle (UAV) system. This UAV is equipped with a standard visible spectral sensor (RGB) and a NovAtel high-precision GNSS positioning module. By connecting to a ground-based augmentation network for Real-Time Kinematic (RTK) services, and integrated with the self-developed professional software UAV Manager, the system supports intelligent flight path planning, multi-source data fusion processing, and automated POS data resolution. During image acquisition, the UAV operated at an altitude of 800 m above the small watershed in terrain-following mode, capturing imagery with an ultra-high spatial resolution of 0.1 m.

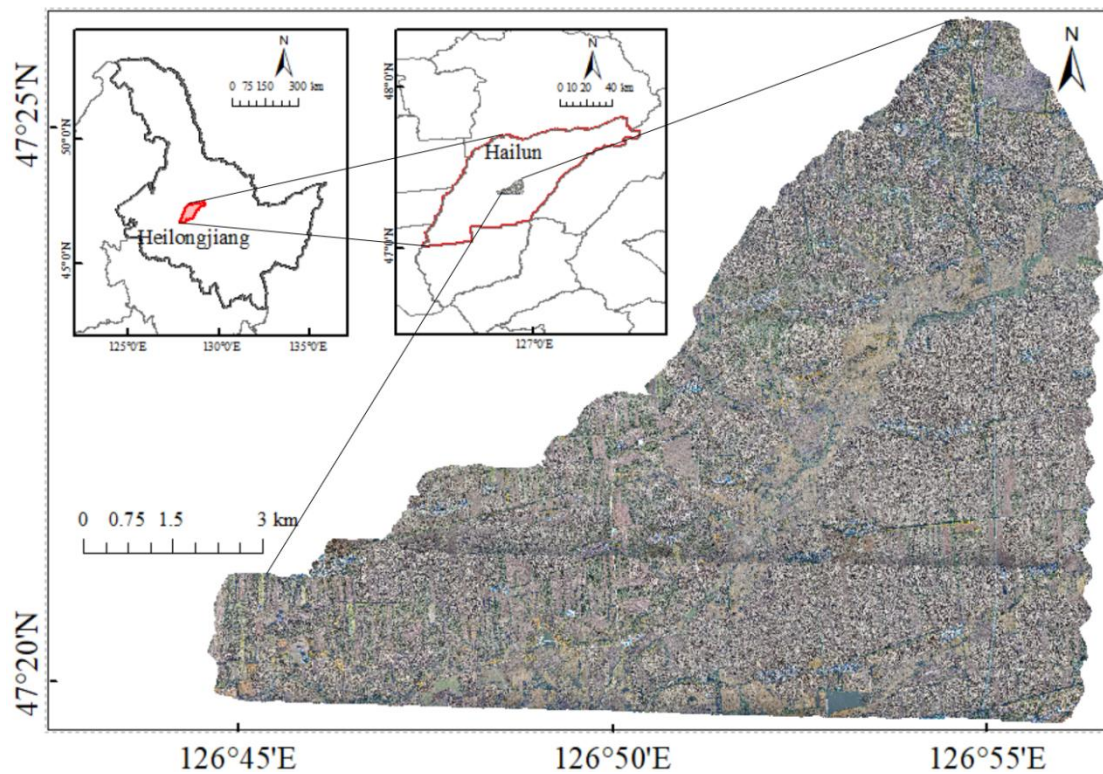


Figure 4 Geographical location and overview of the study area in the Hailun River Basin, Heilongjiang Province, China.

4.2 Data Set Creation

One of the central objectives of the QuESSA (Quantification of Ecological Services for Sustainable Agriculture) project in Europe was to accurately identify the main types of non-cropped habitats within agricultural landscapes and to establish a

classification system with broad applicability across the European continent (Holland et al. 2020). In this study, sampling was conducted in late September—a period when crops have not yet been harvested and vegetation characteristics are most discernible. Following the classification framework developed by the QuESSA project, and based on the key attributes of cropped and non-cropped habitats in the mollisol core region of Northeast China (Hailun City), we developed and validated a habitat dataset applicable to autumn farming systems in this area. The specific habitat types and their principal characteristics are detailed in Table 1.

Table 1 Classification and main characteristics of habitat types in cultivated land system.

Habitat classification	Primary category	Secondary classification	English abbreviation	Main characteristics (end of September)	
Cultivated habitats	Cultivated land	Paddy field	Pf	The field is well-organized; mature rice fields appear golden or yellowish-brown, with clear ridges, minimal standing water, and visible harvesting marks.	
		Dry land	Dl	Dark yellowish-brown tones with clear ridges; crops mature (yellowish-green speckled) or harvested (bare soil/soil stubble)	
Non-cultivated habitats		Woody area	Wa	Foliage dark green (evergreen) or yellowish-green (deciduous); high canopy density, rough texture, distinct shadows	
		Forest belt	Fb	Stratified dark green (evergreen) or yellowish green (deciduous), with clear borders	
		Arbor-Shrub			
		Forest	-Grass compound	Asg	A composite zone of trees, shrubs and herbaceous vegetation; the image tone texture is uneven, dark green and yellow green are interlaced, and the structure is complex
			land		
			Scattered trees	St	Scattered individual or small cluster trees in non-forest background, dark green (evergreen) or yellow-green (deciduous) dot or small patch characteristics
			Grass belt	Gb	Herbaceous vegetation with elongated stripes; the image appears yellow-green or yellow-brown with uniform texture
	Grass				
		Tidal flats	Tf	The transitional zone between high and low water levels; when the water level is low, the sediment is exposed, and the image appears grayish-white, in strip or patch form	
		River	River	A linear or narrow strip of water; the image appears dark blue, with yellowish-brown withered grass and grayish-white mudflats visible along the shore	
	Water area			Stagnant or slow-moving water bodies such as ponds and reservoirs appear dark blue in the image, with visible shoreline vegetation and exposed shallow water forming a tidal flat.	
		Water	Water		
	Other	Paved road	Pr	Artificially paved cement or hardened pavement; images appear bright white or light	

		grey, with regular lines and clear boundaries, no vegetation cover on the pavement
Dirt road	Dr	The unpaved dirt road is used for agricultural machinery; the image is light brown with a small amount of vegetation and clear wheel tracks
Construction land	Cl	Village, highway, factory and other artificial construction areas, image tone complex, geometric shape regular, texture rough
Unused land	Ul	Wasteland (large yellowish brown), saline-alkali land (gray and white), sandy land (bright white), bare land (light brown)
Ridge	Ridge	Narrow earthen ridges used for boundary demarcation and water storage in paddy fields appear light brown or grayish-white, clearly and regularly visible against the field background.

To enhance the generalization capability and robustness of the recognition model under diverse imaging conditions, we implemented a comprehensive set of data augmentation strategies on the collected samples during the training phase. As illustrated in the figure, the augmentation techniques include: (a) original images as the baseline; (b) horizontal flipping to introduce left-right invariance; (c) vertical flipping to simulate inverted viewpoints; (d) random 90-degree rotations to improve orientation invariance. Furthermore, more complex transformations were applied, such as (e) affine transformations to emulate perspective variations; (f) Gaussian blurring to reduce sensitivity to high-frequency noise; (g) Contrast-Limited Adaptive Histogram Equalization (CLAHE) to enhance local contrast under uneven illumination; and (h) HSV color space shifts to address chromatic variations caused by lighting and sensor differences. Collectively, these augmentation methods significantly expand the effective training dataset and improve the model's ability to handle diverse variations in real-world scenarios.

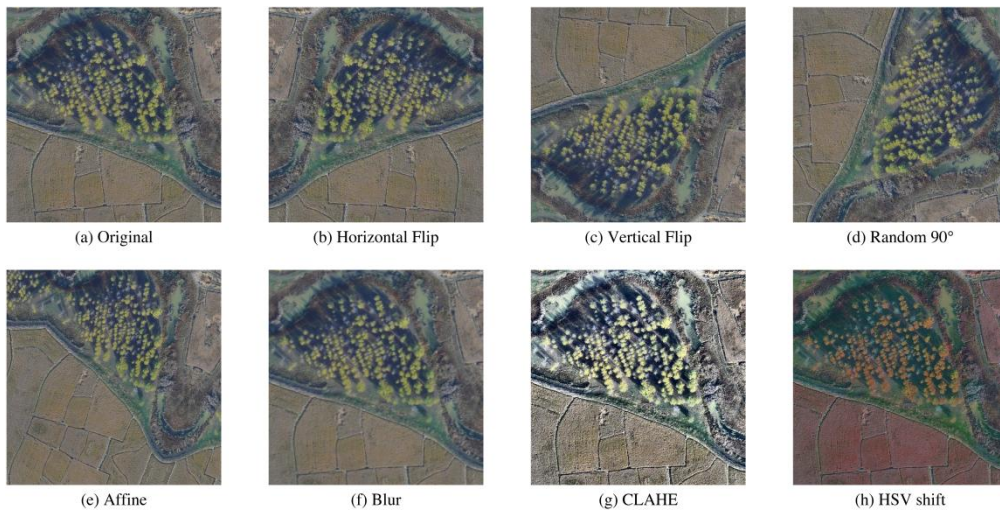


Figure 5 Illustration of data augmentation strategies applied to the training dataset.

4.3 Experimental Environment and Training Parameters

Our proposed framework was implemented based on PyTorch and PyTorch Lightning. Training was conducted using a batch size of 4 ,However, based on this, gradient accumulation was performed every 8 rounds, resulting in an effective batch size of 32. distributed over double RTX 2080Ti 11G GPUs. To accelerate training, we leveraged mixed-precision training (FP16 mixed-precision) throughout the experiments.

During the training process, we utilized the pre-trained DINOv3-ViT-L/16 model with frozen weights. We divided the dataset of 800 total records into train, val, and test sets in a 6:1:1 ratio. For the DWFF-Net, we extracted features from Transformer blocks $\{1, 8, 16, 24\}$. The fusion channel dimension C_{fus} was set to 512. The patch dimensions of the feature map (H_p, W_p) was set to (1248,1248).All models were trained for 150 epochs using the AdamW optimizer with a cosine-annealed learning rate. Standard augmentations including random cropping, flipping, and rotation were employed.

4.4 Weighted Entropy Research

In Figure 6, we selected three high-entropy and three low-entropy images, extracted their corresponding weights from the multi-layer fusion module of the DWFF-Net model, and plotted the weight histograms for different layers along with their weight entropy values. As shown in panels (a), (b), and (c), images containing fewer habitat types exhibit higher weight entropy. Conversely, panels (d), (e), and (f) demonstrate that images with richer habitat feature information correspond to lower weight entropy.

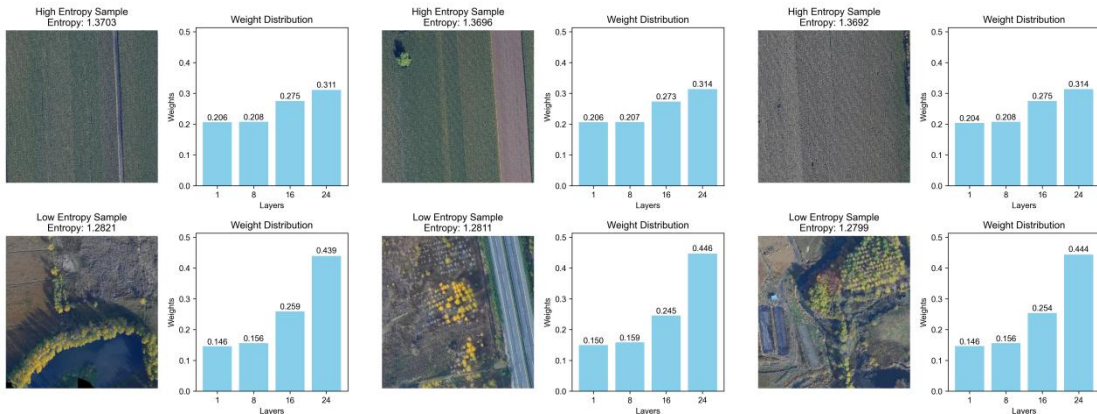


Figure 6 Histograms of layer-wise weights and corresponding entropy values for high-entropy and low-entropy images.

We investigated the relationship between weight entropy and the number of habitat categories present in the images. As shown in the figure, as the number of habitat features in an image increases, the weight entropy exhibits a decreasing trend.

This phenomenon indicates that when an image contains more diverse habitat categories and richer feature information, the model's weight assignment across layers in the multi-layer fusion module becomes more concentrated and stable. From a data-driven perspective, this implies that the model can automatically adjust layer-wise weights based on the actual number of habitat features present in the image, thereby better capturing and integrating key information. When the number of habitat features is limited, the model may need to more broadly explore and balance the contributions of different layers in the multi-layer fusion module, leading to a more dispersed weight distribution and consequently higher weight entropy. In contrast, as the number of habitat features increases, the model becomes more capable of identifying critical features and allocating greater weight to the relevant layers, resulting in a more focused weight distribution and a corresponding decrease in weight entropy.

We speculate that the relationship between weight entropy and the number of habitat categories may reflect the model's adaptive capability in handling data of varying complexity. In practical applications, this characteristic enables the model to utilize feature information from different layers more effectively when confronted with complex and diverse habitat scenarios, thereby improving the accuracy of habitat type recognition.

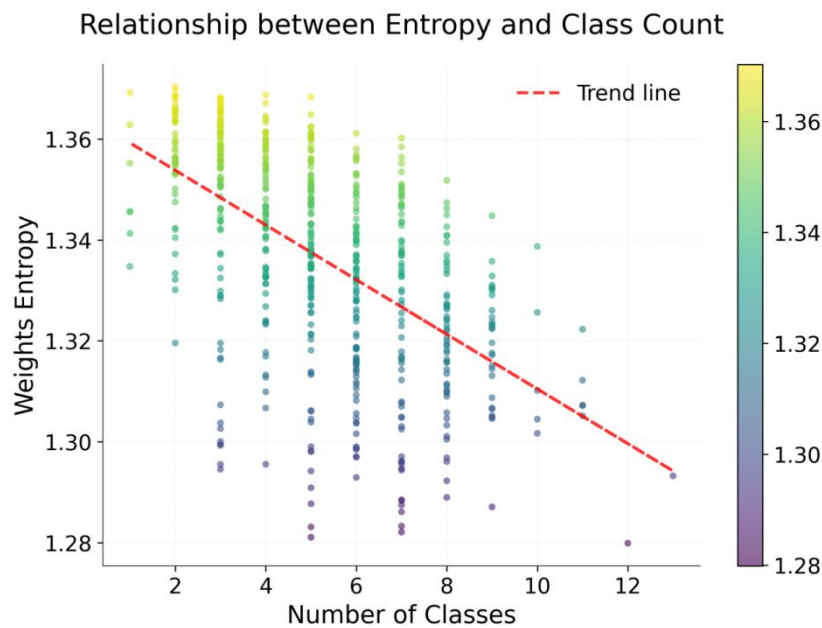


Figure 7 Relationship between weight entropy and the number of habitat categories present in images.

Furthermore, the overall distribution of weight entropy was visualized using a histogram, which revealed a broader spread in the high-entropy region and a more concentrated distribution in the low-entropy region. This pattern indicates variations in the model’s ability to handle habitat features of differing complexity. The widespread distribution in the high-entropy region may reflect that when processing images with relatively homogeneous and less informative habitat features, the model requires more exploration and adaptation, leading to increased uncertainty in weights and a more dispersed entropy distribution. In contrast, the concentrated distribution in the low-entropy region suggests that when images contain diverse and rich habitat features, the model can determine layer weights more efficiently, resulting in relatively stable and focused weight entropy.

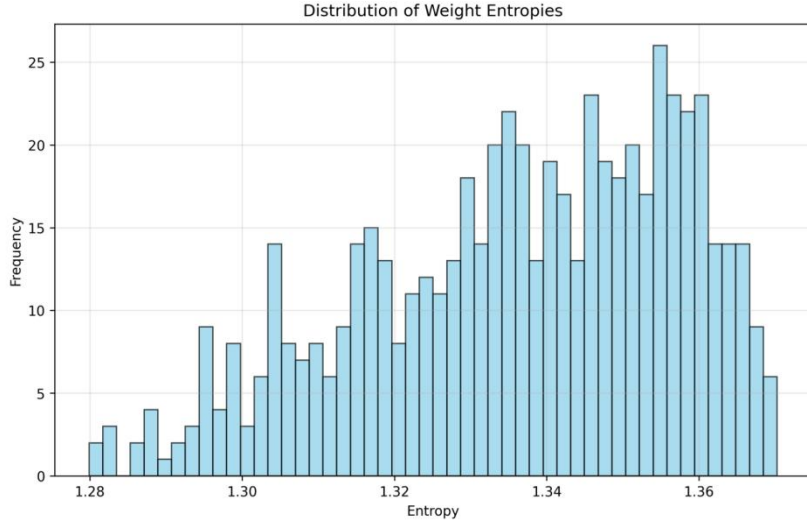


Figure 8 Histogram of the overall distribution of weight entropy values.

Through an in-depth investigation of the weight entropy distribution, we not only elucidate the adaptive mechanisms of the model in processing data from habitats with varying complexities, but also provide a critical foundation for further model optimization. In future research, targeted refinements can be made based on the characteristics of the weight entropy distribution. For instance, the structure of the multi-layer fusion module could be adjusted, or the strategy for weight allocation could be optimized, thereby enhancing the model's recognition performance across diverse habitat scenarios.

4.5 Ablation Studies

To rigorously validate the contribution of each component in the proposed framework, we conducted comprehensive ablative experiments. The baseline model employs a non-weighted multi-layer feature fusion network, termed Non-weighted Feature Fusion Network with L layers (NWFF-Net-L), where L denotes the number of

fused layers. For comparison, a Static Weighted Feature Fusion Network (SWFF-Net) was also established to verify the effectiveness of dynamic weight-based fusion. Throughout the ablation studies, the core innovation of this work—a multi-layer feature fusion network with dynamic weighting—was progressively integrated. All models were trained and evaluated on the same dataset dataset under identical experimental configurations, including learning rate, optimizer, and number of training epochs. Quantitative results are detailed in Table 2.

Table 2 Ablation study results comparing different feature fusion strategies.

Method	mPrecision	mRecall	mF1	mIoU
NWFF-Net-1	0.7831	0.7992	0.7888	0.6763
NWFF-Net-2	0.7888	0.8032	0.7946	0.6844
NWFF-Net-3	0.7772	0.7956	0.7843	0.6723
NWFF-Net-4	0.7822	0.7946	0.787	0.6771
SWFF-Net	0.7925	0.7944	0.7925	0.6852
DWFF-Net	0.8006	0.8131	0.8049	0.6979

As shown in Table 2, the baseline model Non-weighted Feature Fusion Network (1 layers) (NWFF-Net-1) has already demonstrated outstanding performance, fully illustrating the advantage of the DINOv3 feature extraction technique. With the introduction of a multi-level feature fusion mechanism incorporating global weighting, the SWFF-Net model achieved a notable improvement in overall mIoU compared to the standard model, with an increase of 0.01. Furthermore, by adopting a dynamic weighting strategy in the multi-level feature fusion mechanism, the DWFF-Net model exhibited an even more significant enhancement in overall mIoU over the SWFF-Net, with a gain of 0.012 percentage points. More importantly, the IoU for the Scattered trees (St) also increased markedly by nine percentage points, further validating that the dynamic integration of shallow texture features and deep semantic features plays a crucial role in fully leveraging multi-level feature information.

Experimental results with the hybrid loss function (Fig. 9) indicate that the DWFF-Net model demonstrates significant performance advantages throughout 150 training iterations. Its final training loss (0.114) was lower than that of the baseline model (0.156), confirming the effectiveness of multi-level feature fusion. Additionally, after 80 iterations, the rate of loss reduction for the DWFF-Net model surpassed that of the SWFF-Net, underscoring the efficacy of the proposed dynamic weighting network in multi-level feature fusion.

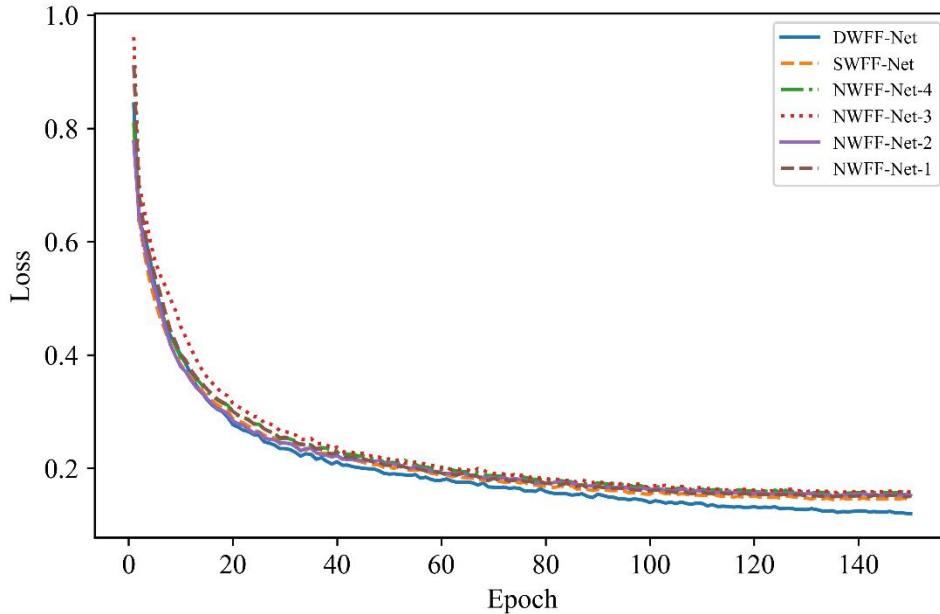


Figure 9 Training loss curves for DWFF-Net, SWFF-Net, and baseline models.

4.6 Comparison Experiment

Finally, we compared the full DWFF-Net framework against several well-established semantic segmentation models. For a fair comparison, All models underwent standard pre-training on our dataset using ImageNet.

Table 3 Performance comparison of DWFF-Net with other semantic segmentation models.

Model	Backbone	mPrecision	mRecall	mF1	mIoU
U-Net ^[4]	ResNet-50	0.7192	0.6756	0.6865	0.584
DeepLabv3+ ^[5]	ResNet-50	0.7873	0.7638	0.7729	0.6526
DWFF-Net (Ours)	Frozen DINOv3-L	0.8006	0.8131	0.8049	0.6979

As demonstrated in Table 3, our DWFF-Net framework substantially outperforms all competing methods by a significant margin. This performance advantage is particularly pronounced in the category of field ridges, where our model leads the second-best method, DeepLabv3+, by 0.6979 IoU points. These results underscore the unique strength of the proposed approach — combining the DINOv3 model with dynamic weight feature fusion — in handling complex informational structures.

As shown by the loss curves in Figure 10, all three models — U-Net, DeepLabV3+, and DWFF-Net — exhibit a converging trend throughout the training process. However, notable differences are observed in terms of convergence speed and final loss values. While the U-Net model requires nearly 100 iterations to approach stability, our proposed DWFF-Net stabilizes after only 60 iterations. By the

end of training, DWFF-Net achieves the lowest final loss, significantly outperforming both DeepLabV3+ (IoU 0.65) and U-Net (IoU 0.58). This further validates the superior performance of the proposed DWFF-Net model.

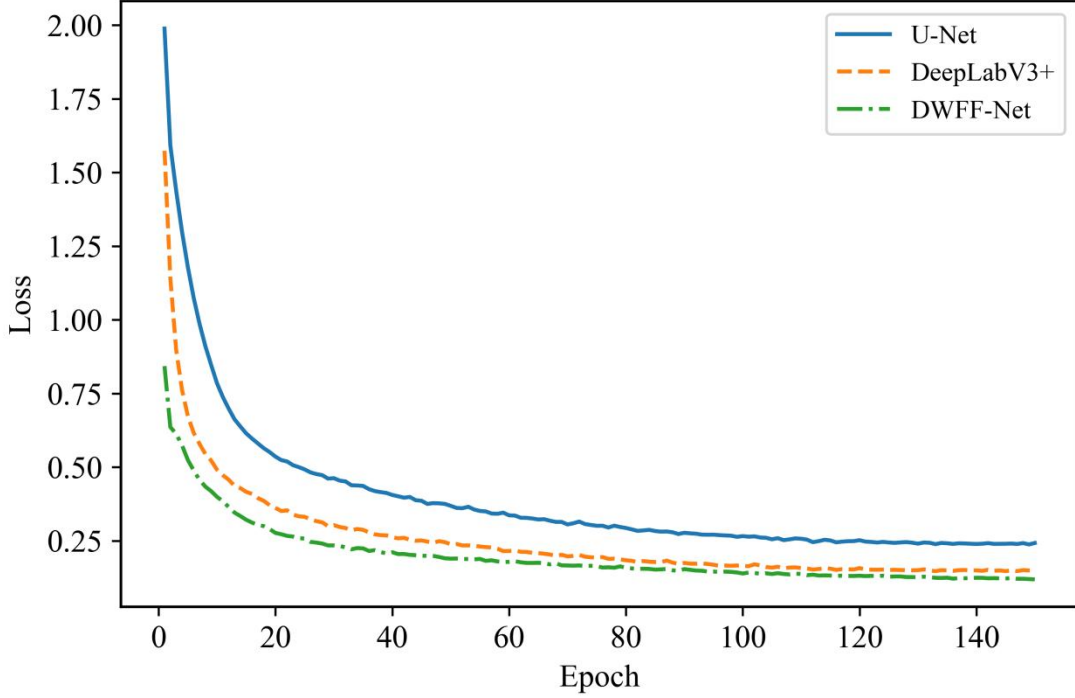


Figure 10 Comparison of training loss curves among U-Net, DeepLabV3+, and DWFF-Net.

4.7 Qualitative Results

The performance of different models — NWFF-Net-L, SWFF-Net, and DWFF-Net — in habitat identification is summarized in Table 4. The results demonstrate a significant improvement in the extraction accuracy of linear features, which play crucial roles in maintaining the ecological functions of cultivated land systems. Specifically, the Intersection over Union (IoU) values for Scattered trees (St) and River canals (River) reached 0.2707 and 0.7626, respectively, demonstrating an improvement of six percentage points compared to conventional single-layer feature identification methods based on NWFF-Net.

Table 4 F1 and IoU values of 15 habitat types in different feature fusion strategies.

Class	NWFF-Net-1		NWFF-Net-2		NWFF-Net-3		NWFF-Net-4		SWFF-Net		DWFF-Net	
	F1	IoU	F1	IoU	F1	IoU	F1	IoU	F1	IoU	F1	IoU
Asg	0.6005	0.4291	0.6273	0.4570	0.6246	0.4541	0.6358	0.4660	0.6181	0.4473	0.6040	0.4326
DI	0.9831	0.9667	0.9833	0.9671	0.9838	0.9681	0.9842	0.9689	0.9841	0.9687	0.9839	0.9682
Gb	0.6426	0.4734	0.6457	0.4768	0.6570	0.4892	0.6322	0.4622	0.6391	0.4696	0.6222	0.4516
St	0.3604	0.2198	0.3781	0.2331	0.3189	0.1897	0.3057	0.1804	0.3059	0.1806	0.4261	0.2707
Dr	0.8243	0.7011	0.8233	0.6997	0.8235	0.6999	0.8145	0.6871	0.8262	0.7038	0.8175	0.6913

Pr	0.9071	0.8300	0.9075	0.8306	0.9182	0.8487	0.9092	0.8336	0.9121	0.8384	0.9098	0.8345
Fb	0.8261	0.7038	0.8235	0.6999	0.8142	0.6866	0.8166	0.6900	0.8330	0.7138	0.8241	0.7008
Wa	0.8639	0.7605	0.8635	0.7597	0.8726	0.7741	0.8703	0.7703	0.8647	0.7616	0.8595	0.7537
Ul	0.7727	0.6296	0.7831	0.6436	0.7787	0.6376	0.7774	0.6358	0.7807	0.6403	0.7825	0.6427
Pf	0.9854	0.9711	0.9861	0.9726	0.9858	0.9721	0.9863	0.9730	0.9865	0.9733	0.9869	0.9741
Ridge	0.7908	0.6540	0.7978	0.6637	0.7890	0.6515	0.7908	0.6540	0.8029	0.6707	0.8127	0.6846
Cl	0.9061	0.8283	0.9064	0.8288	0.9086	0.8325	0.9105	0.8357	0.9112	0.8368	0.9088	0.8328
River	0.7713	0.6278	0.8186	0.6928	0.7615	0.6149	0.8160	0.6892	0.8299	0.7092	0.8653	0.7626
Tf	0.7069	0.5467	0.6541	0.4860	0.6470	0.4782	0.6472	0.4784	0.6643	0.4974	0.7175	0.5594
Water	0.8906	0.8027	0.9214	0.8543	0.8813	0.7877	0.9083	0.8320	0.9287	0.8668	0.9523	0.9090

Figure 11 provides a visual comparison of the segmentation results on challenging test images. It is evident that while baseline methods like NWFF-Net and SWFF-Net produce noisy and heavily fragmented predictions for the field ridges, our DWFF-Net generates remarkably clean, continuous, and accurate segmentation maps. The topological structure of the field network is well-preserved, which is a direct result of the components working in concert.

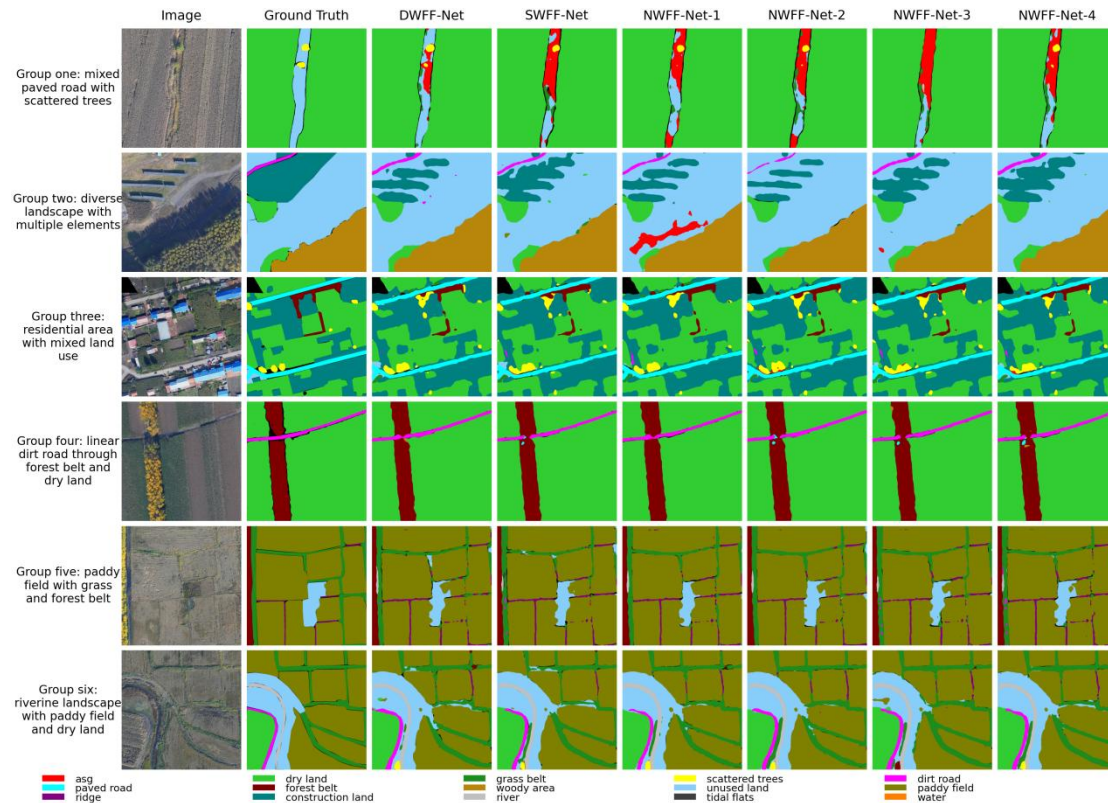


Figure 11 Comparison of extraction effects of DWFF-Net, SWFF-Net and different NWFF-Net.

Table 5 summarizes the habitat recognition performance of the U-Net, DeepLabV3+, and DWFF-Net models. The results demonstrate a significant

improvement in the extraction accuracy of linear landscape features, which play a critical role in maintaining the ecological functions of cultivated land systems. Specifically, the Intersection over Union (IoU) scores for Paved roads (Pr) and River reached 0.8345 and 0.7626, respectively, representing a notable increase of compared to the conventional interpretation method based on U-Net.

Table 5 F1 and IoU values of 15 habitat types in U-Net, DeepLabv3+, and DWFF-Net.

Class	U-Net		DeepLabv3+		DWFF-Net	
	F1	IoU	F1	IoU	F1	IoU
Asg	0.5958	0.4243	0.6645	0.4975	0.6040	0.4326
DI	0.9754	0.9521	0.9813	0.9632	0.9839	0.9682
Gb	0.5597	0.3886	0.6271	0.4568	0.6222	0.4516
St	0.0008	0.0004	0.3867	0.2397	0.4261	0.2707
Dr	0.7783	0.6370	0.7681	0.6236	0.8175	0.6913
Pr	0.9057	0.8276	0.8907	0.8029	0.9098	0.8345
Fb	0.7585	0.6109	0.8065	0.6757	0.8241	0.7008
Wa	0.8469	0.7345	0.8797	0.7853	0.8595	0.7537
UI	0.7714	0.6279	0.7749	0.6326	0.7825	0.6427
Pf	0.9732	0.9477	0.9698	0.9414	0.9869	0.9741
Ridge	0.0000	0.0000	0.7769	0.6353	0.8127	0.6846
CI	0.8864	0.7960	0.9013	0.8204	0.9088	0.8328
River	0.7013	0.5400	0.7160	0.5577	0.8653	0.7626
Tf	0.6895	0.5262	0.6234	0.4529	0.7175	0.5594
Water	0.8554	0.7473	0.8259	0.7034	0.9523	0.9090

Figure 12 provides a visual comparison of the segmentation results on challenging test images. It is evident that while baseline methods like U-Net and DeepLabv3+ produce noisy and heavily fragmented predictions for the field ridges, our DWFF-Net generates remarkably clean, continuous, and accurate segmentation maps. The topological structure of the field network is well-preserved, which is a direct result of the DINOv3 and Dynamic-Weighted Feature Fusion Net components working in concert.

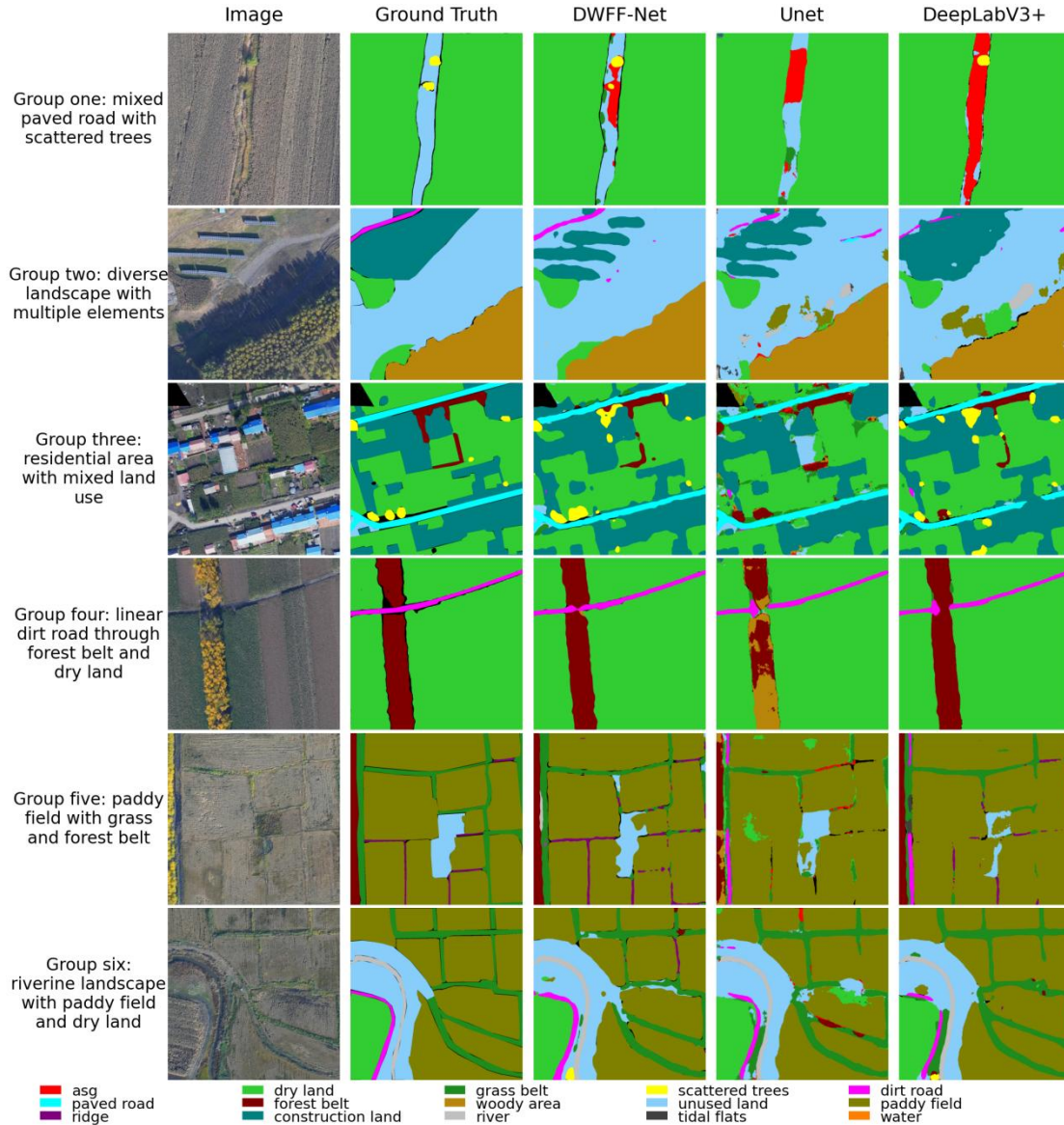


Figure 12 Comparison of extraction effects of DWFF-Net, U-net and DeepLabV3+.

This study introduces a high-accuracy identification method (the DWFF-Net model), which significantly enhances two key aspects of the traditional cultivated land system habitat classification framework: first, it mitigates the "blurring effect" along land-use boundaries, as evidenced by improved recognition accuracy in transition zones between Construction land (IoU 0.8328) and Unused land (IoU 0.6427); second, it substantially reduces the "omission phenomenon" in fragmented patches, increasing the detection rate of micro-habitats from 0.5840 with conventional methods to 0.6979. Based on centimeter-level precision imagery, the model and fine-grained classification system developed in this study provide a meter-level delineation scheme and a reference classification standard for the accurate identification of cultivated land system habitats at larger scales.

5. Discussion

In the comparative evaluation of feature recognition across different categories, the DWFF-Net model demonstrated outstanding performance for all categories except field ridges, including Asg, Dl, and Gb. Experimental results showed that DWFF-Net outperformed models like NWFF-Net, SWFF-Net, U-Net, and DeepLabv3+ in key metrics such as F1, Precision, Recall, and IoU.

Taking the Asg category as an example, while other models exhibit prediction biases and instability, the DWFF-Net model demonstrates superior accuracy in identifying its features. It achieves high F1, Precision, and Recall values, with an IoU score of 0.4326 that significantly outperforms competing models. This indicates DWFF-Net's capability to precisely segment Asg-related regions in images, effectively reducing both false positives and false negatives.

In other categories such as Gb and St, DWFF-Net also demonstrates similar advantages. It effectively integrates multi-level feature information and dynamically adjusts weights based on category-specific characteristics, achieving efficient recognition and accurate segmentation of various features. This advantage is not only reflected in quantitative metrics but also visually evident from the recognition results. When handling complex test images, other models may produce segmented results with excessive noise and fragments, whereas DWFF-Net consistently generates clean, continuous, and accurate segmentation maps that preserve the topological structure of category-specific features.

Compared to existing models such as U-Net and DeepLabv3+, the proposed model exhibits higher computational complexity, resulting in longer training time. Furthermore, its capability to resolve dynamic changes in video sequences remains limited. In future work, we intend to incorporate lightweight network architectures to enhance computational and inference efficiency, thereby improving the model's overall performance in video analysis tasks.

In summary, the comparative analysis of feature recognition across different categories has thoroughly validated the effectiveness and superiority of the proposed DWFF-Net model in semantic segmentation tasks, providing robust support for research and applications in related fields.

6. Conclusion

This study introduces an innovative framework named DWFF-Net, specifically designed for fine-grained semantic segmentation of agricultural drone imagery. By

incorporating a data-driven dynamic weight feature fusion mechanism and a hybrid regularization loss function enhanced with weighted entropy, we successfully adapt the powerful DINOv3 vision foundation model to the challenging task of remote sensing, while keeping the backbone network frozen. Comprehensive comparative experiments demonstrate that DWFF-Net outperforms mainstream segmentation models across multiple key metrics. Overall, DWFF-Net achieves an mIoU of 0.6979, surpassing well-established models such as U-Net (mIoU 0.584) and DeepLabv3+ (mIoU 0.6526). In the segmentation of fine-grained habitats, DWFF-Net also exhibits superior performance. For instance, in identifying Scattered trees (St) and Dirt roads (Dr), DWFF-Net achieves IoU scores of 0.2707 and 0.6913, respectively, outperforming U-Net (IoU 0.0004; 0.6370) and DeepLabv3+ (IoU 0.2397; 0.6236). These results validate the excellent performance of our DINOv3-based DWFF-Net model in habitat system segmentation. Furthermore, ablation studies confirm the effectiveness of the dynamic weight feature fusion mechanism in improving recognition accuracy. Overall, DWFF-Net (mIoU 0.6979) surpasses SWFF-Net (mIoU 0.6852). In segmenting fine-grained habitats, DWFF-Net also outperforms the globally weighted multi-layer fusion model SWFF-Net. For example, in identifying Scattered trees (St) and Rivers (River), DWFF-Net achieves IoU scores of 0.2707 and 0.7626, respectively, exceeding those of SWFF-Net (IoU 0.1806; 0.7092). Our work not only establishes a new benchmark on the evaluation dataset but also paves the way for broader application of vision foundation models in specialized domains such as precision agriculture.

CRedit authorship contribution statement

Kesong Zheng: Writing – review & editing, Methodology, Investigation, Formal analysis. Zhi Song: Writing – review & editing, Methodology, Investigation, Formal analysis. Peizhou Li: Writing – review & editing, Writing – original draft, Visualization, Methodology, Investigation, Formal analysis. Shuyi Yao: Writing – review & editing, Methodology, Investigation, Formal analysis. Zhenxing Bian: Writing – review & editing, Writing – original draft, Visualization, Methodology, Investigation, Funding acquisition, Formal analysis, Conceptualization.

Declaration of competing interests

The authors declare that they have no known competing financial interests or personal relationships that could have appeared to influence the work reported in this paper.

Acknowledgments

This research was supported by the Scientific Research Fund of Liaoning Provincial Education Department of China under [Grant number LJ212510157036].

Data availability

The data that has been used is confidential. The complete code repository can be accessed via GitHub at the following URL: <https://github.com/sysau/DWFF-Net>

References

- Azad, Reza, Ehsan Khodapanah Aghdam, Amelie Rauland, Yiwei Jia, Atlas Haddadi Avval, Afshin Bozorgpour, Sanaz Karimijafarbigloo, Joseph Paul Cohen, Ehsan Adeli, and Dorit Merhof. 2024. "Medical Image Segmentation Review: The Success of U-Net." *IEEE Transactions on Pattern Analysis and Machine Intelligence* 46(12):10076–95. doi:10.1109/TPAMI.2024.3435571.
- Cao, Qianyang, Man Li, Guangbin Yang, Qian Tao, Yaopei Luo, Renru Wang, and Panfang Chen. 2024. "Urban Vegetation Classification for Unmanned Aerial Vehicle Remote Sensing Combining Feature Engineering and Improved DeepLabV3+." *Forests* 15(2). doi:10.3390/f15020382.
- Chen, Liang-Chieh, Yukun Zhu, George Papandreou, Florian Schroff, and Hartwig Adam. 2018. "Encoder-Decoder with Atrous Separable Convolution for Semantic Image Segmentation." Pp. 833–51 in *Computer Vision – ECCV 2018*, edited by V. Ferrari, M. Hebert, C. Sminchisescu, and Y. Weiss. Cham: Springer International Publishing.
- Delabre, Izabela, Lily O. Rodriguez, Joanna Miller Smallwood, Jorn P. W. Scharlemann, Joseph Alcamo, Alexander S. Antonarakis, Pedram Rowhani, Richard J. Hazell, Dag L. Aksnes, Patricia Balvanera, Carolyn J. Lundquist, Charlotte Gresham, Anthony E. Alexander, and Nils C. Stenseth. 2021. "Actions on Sustainable Food Production and Consumption for the Post-2020 Global Biodiversity Framework." *Science Advances* 7(12). doi:10.1126/sciadv.abc8259.
- Fan, Junfu, Zongwen Shi, Zhoupeng Ren, Yuke Zhou, and Min Ji. 2024. "DDPM-SegFormer: Highly Refined Feature Land Use and Land Cover Segmentation with a Fused Denoising Diffusion Probabilistic Model and Transformer." *International Journal of Applied Earth Observation and Geoinformation* 133:104093. doi:10.1016/j.jag.2024.104093.
- Farhangfar, Saghar, and Mehdi Rezaeian. 2019. "Semantic Segmentation of Aerial Images Using FCN-Based Network." Pp. 1864–68 in *2019 27th Iranian Conference on Electrical Engineering (ICEE)*.

- Guo, Xiaoyu, Zhenxing Bian, Shuai Wang, Qiubing Wang, Yufei Zhang, Jun Zhou, and Lin Lin. 2020. "Prediction of the Spatial Distribution of Soil Arthropods Using a Random Forest Model: A Case Study in Changtu County, Northeast China." *Agriculture, Ecosystems & Environment* 292:106818. doi:10.1016/j.agee.2020.106818.
- Holland, John M., Philippe Jeanneret, Anna-Camilla Moonen, Wopke van der Werf, Walter A. H. Rossing, Daniele Antichi, Martin H. Entling, Brice Giffard, Herman Helsen, Mark Szalai, Carlo Rega, Caroline Gibert, and Eve Veromann. 2020. "Approaches to Identify the Value of Seminatural Habitats for Conservation Biological Control (Vol 11, Pg 195, 2020)." *Insects* 11(5). doi:10.3390/insects11050272.
- Jingping, Liu, Jin Xiaobin, Han Bo, Lin Jinhuang, Zhang Xiaolin, Liang Xinyuan, and Zhou Yinkang. 2022. "Connotation, Characteristics and Recognition of Semi-Natural Habitats in Agricultural Space." *Shengtai Xuebao* 42(22):9199–9212.
- Kalchbrenner, Nal, Edward Grefenstette, and Phil Blunsom. 2014. "A Convolutional Neural Network for Modelling Sentences." Pp. 655–65 in *Proceedings of the 52nd Annual Meeting of the Association for Computational Linguistics (Volume 1: Long Papers)*, edited by K. Toutanova and H. Wu. Baltimore, Maryland: Association for Computational Linguistics.
- Li, Juanhui, Sreyashi Nag, Hui Liu, Xianfeng Tang, Sheikh Sarwar, Limeng Cui, Hansu Gu, Suhang Wang, Qi He, and Jiliang Tang. 2025. "Learning with Less: Knowledge Distillation from Large Language Models via Unlabeled Data."
- Liu, Han, and Peng Gong. 2021. "21st Century Daily Seamless Data Cube Reconstruction and Seasonal to Annual Land Cover and Land Use Dynamics Mapping-iMap (China) 1.0." *National Remote Sensing Bulletin* 25(Compindex):126–47. doi:10.11834/jrs.20210580.
- Peng, Fengcan, Qiuzhi Peng, Di Chen, Jiating Lu, and Yufei Song. 2024. "Extraction of Terraces in Hilly Areas from Remote Sensing Images Using DEM and Improved U-Net." *Photogrammetric Engineering and Remote Sensing* 90(3). doi:10.14358/PERS.23-00069R2.
- Qiao, Yicheng, Wei Liu, Bin Liang, Pengyun Wang, Haopeng Zhang, and Junli Yang. 2023. "SeMask-Mask2Former: A Semantic Segmentation Model for High Resolution Remote Sensing Images." Pp. 1–6 in *2023 IEEE Aerospace Conference*.
- Sheppard, Clay, and Maryam Rahnemoonfar. 2017. "Real-Time Scene Understanding for UAV Imagery Based on Deep Convolutional Neural Networks." Pp. 2243–46 in *2017 IEEE INTERNATIONAL GEOSCIENCE AND REMOTE*

SENSING SYMPOSIUM (IGARSS), IEEE International Symposium on Geoscience and Remote Sensing IGARSS. Fort Worth, TX: IEEE.

- Siméoni, Oriane, Huy V. Vo, Maximilian Seitzer, Federico Baldassarre, Maxime Oquab, Cijo Jose, Vasil Khalidov, Marc Szafraniec, Seungeun Yi, Michaël Ramamonjisoa, Francisco Massa, Daniel Haziza, Luca Wehrstedt, Jianyuan Wang, Timothée Darcet, Théo Moutakanni, Leonel Sentana, Claire Roberts, Andrea Vedaldi, Jamie Tolan, John Brandt, Camille Couprie, Julien Mairal, Hervé Jégou, Patrick Labatut, and Piotr Bojanowski. 2025. “DINOv3.”
- Song, Pengfei, Jinjiang Li, Zhiyong An, Hui Fan, and Linwei Fan. 2023. “CTMFNet: CNN and Transformer Multiscale Fusion Network of Remote Sensing Urban Scene Imagery.” *IEEE Transactions on Geoscience and Remote Sensing* 61:1–14. doi:10.1109/TGRS.2022.3232143.
- Sumbul, Gencer, Arne de Wall, Tristan Kreuziger, Filipe Marcelino, Hugo Costa, Pedro Benevides, Mario Caetano, Begum Demir, and Volker Markl. 2021. “BigEarthNet-MM A Large-Scale, Multimodal, Multilabel Benchmark Archive for Remote Sensing Image Classification and Retrieval.” *Ieee Geoscience and Remote Sensing Magazine* 9(3):174–80. doi:10.1109/MGRS.2021.3089174.
- Tougeron, Kevin, Eloise Couthouis, Ronan Marrec, Lena Barascou, Jacques Baudry, Hugues Boussard, Francoise Burel, Aude Couty, Geraldine Doury, Charlotte Francis, Florence Hecq, Vincent Le Roux, Julien Petillon, Fabien Spicher, Thierry Hance, and Joan van Baaren. 2022. “Multi-Scale Approach to Biodiversity Proxies of Biological Control Service in European Farmlands.” *Science of the Total Environment* 822. doi:10.1016/j.scitotenv.2022.153569.
- Tulczyjew, Lukasz, Michal Kawulok, Nicolas Longépé, Bertrand Le Saux, and Jakub Nalepa. 2022. “Graph Neural Networks Extract High-Resolution Cultivated Land Maps from Sentinel-2 Image Series.” *IEEE Geoscience and Remote Sensing Letters* 19:1–5. doi:10.1109/LGRS.2022.3185407.
- Vaswani, Ashish, Noam Shazeer, Niki Parmar, Jakob Uszkoreit, Llion Jones, Aidan N. Gomez, Łukasz Kaiser, and Illia Polosukhin. n.d. “Attention Is All You Need.”
- Wang, Chuqiao, Zhenxing Bian, Yufei Zhang, and Deyang Guan. 2024. “Direct and Indirect Effects of Linear Non-Cultivated Habitats on Epigaeic Macroarthropod Assemblages.” *Ecological Indicators* 160:111871. doi:10.1016/j.ecolind.2024.111871.
- Yuan, Xiaohui, Jianfang Shi, and Lichuan Gu. 2021. “A Review of Deep Learning Methods for Semantic Segmentation of Remote Sensing Imagery.” *Expert Systems with Applications* 169:114417. doi:10.1016/j.eswa.2020.114417.

- Zhang, Yufei, Zhenxing Bian, Xiaoyu Guo, and Chuqiao Wang. 2025. "Multiscale Agrobiodiversity Conservation: Modeling Epigaeic Arthropod Diversity with Landscape Heterogeneity and Ecosystem Services." *Journal of Environmental Management* 388(Compendex). doi:10.1016/j.jenvman.2025.126003.
- Zhang, Yufei, Zhenxing Bian, Shuai Wang, Xiaoyu Guo, and Wei Zhou. 2024. "Effect of Agricultural Landscape Pattern on the Qualitative Food Web of Epigaeic Arthropods in Low Hilly Areas of Northern China." *Ecological Modelling* 488:110574. doi:10.1016/j.ecolmodel.2023.110574.
- Zhang, Zhen, Lehao Huang, Qingwang Wang, Linhuan Jiang, Yemao Qi, Shunyuan Wang, Tao Shen, Bo-Hui Tang, and Yanfeng Gu. 2025. "UAV Hyperspectral Remote Sensing Image Classification: A Systematic Review." *IEEE Journal of Selected Topics in Applied Earth Observations and Remote Sensing* 18:3099–3124. doi:10.1109/JSTARS.2024.3522318.
- Zhang, Zhibo, Xining Zhao, Haichen Jiang, Hao Yuan, Long Yang, Xiaodong Gao, Liangliang Shi, and Yuting Niu. 2022. "Precise Classification of Land Use in Weibei Dryland Using UAV Images and Deep Learning." *Nongye Gongcheng Xuebao/Transactions of the Chinese Society of Agricultural Engineering* 38(Compendex):199–209. doi:10.11975/j.issn.1002-6819.2022.22.022.
- Zhou, P., G. Cheng, X. Yao, and J. Han. 2021. "Machine Learning Paradigms in High-Resolution Remote Sensing Image Interpretation." *Yaogan Xuebao/Journal of Remote Sensing* 25:182–97. doi:10.11834/jrs.20210164.
- Zualkernan, Imran, Daa Addeen Abuhani, Maya Haj Hussain, Jowaria Khan, and Mohamed ElMohandes. 2023. "Machine Learning for Precision Agriculture Using Imagery from Unmanned Aerial Vehicles (UAVs): A Survey." *Drones* 7(6). doi:10.3390/drones7060382.